

Intrinsically disordered proteins aggregate at fungal cell-to-cell channels and regulate intercellular connectivity

Julian Lai^{a,b}, Chuan Hock Koh^{c,d}, Monika Tjota^{a,b}, Laurent Pieuchot^{a,b}, Vignesh Raman^{a,b}, Karthik Balakrishna Chandrababu^b, Daiwen Yang^b, Limsoon Wong^c, and Gregory Jedd^{a,b,1}

^aTemasek Life Sciences Laboratory and ^bDepartment of Biological Sciences, National University of Singapore, Singapore 117604; ^cSchool of Computing, National University of Singapore, Singapore 117417; and ^dGraduate School for Integrative Sciences and Engineering, National University of Singapore, Singapore 117597

Edited by Han A. B. Wosten, Utrecht University, Utrecht, The Netherlands, and accepted by the Editorial Board August 7, 2012 (received for review May 10, 2012)

Like animals and plants, multicellular fungi possess cell-to-cell channels (septal pores) that allow intercellular communication and transport. Here, using a combination of MS of Woronin body-associated proteins and a bioinformatics approach that identifies related proteins based on composition and character, we identify 17 septal pore-associated (SPA) proteins that localize to the septal pore in rings and pore-centered foci. SPA proteins are not homologous at the primary sequence level but share overall physical properties with intrinsically disordered proteins. Some SPA proteins form aggregates at the septal pore, and in vitro assembly assays suggest aggregation through a nonamyloid mechanism involving mainly α -helical and disordered structures. SPA loss-of-function phenotypes include excessive septation, septal pore degeneration, and uncontrolled Woronin body activation. Together, our data identify the septal pore as a complex subcellular compartment and focal point for the assembly of unstructured proteins controlling diverse aspects of intercellular connectivity.

multicellular organization | filamentous fungus | *Neurospora crassa*

Two distinct strategies provide the foundation for eukaryotic multicellular organization. Animals use cell-to-cell adhesion to maintain tissue architecture, whereas rigid cell walls and lack of cell separation following cytokinesis retain plants in precise 3D arrangements (1, 2). Fungi use both strategies; lack of separation after cytokinesis allows the production of multicellular filaments known as hyphae, which can further aggregate in a developmentally regulated manner to make fruiting bodies. Channels that bridge adjacent cells play diverse roles in multicellular tissues. In plants, plasmodesmata not only support systemic transport of small molecular nutrients and hormones but allow cell-to-cell trafficking of transcription factors, and this plays an important role in cell fate determination (reviewed in 3, 4). In animals, gap junctions permit the exchange of ions and small signaling molecules, allowing cells to coordinate their development and activity, as seen, for example, in heart muscle (reviewed in 5).

Fungal hyphae grow by tip extension, and apical cells periodically produce cell walls (septa) that partition the growing hypha into compartments. Septa typically possess a single, centrally located pore, which allows intercellular transport and, in some cases, bulk flow of protoplasm. This arrangement, central to the fungal lifestyle, allows cells to cooperate and promotes rapid invasive and foraging growth of symbiotic, saprotrophic, and pathogenic fungi alike. Depending on environmental and developmental cues, hyphae aggregate to make complex spore-dispersing fruiting bodies (6). In fungal groups forming these structures, septal pores harbor membrane-bound organelles: peroxisomal Woronin bodies in the Ascomycota, and the endoplasmic reticulum-derived septal pore cap (SPC) in the Basidiomycota (7, 8).

Septal pores provide advantages but also make hyphal networks especially vulnerable to cellular damage, and both the SPC and Woronin body perform an adaptive function to ameliorate this risk. When the hypha is damaged, Woronin bodies occlude

the pore of nearby septa to limit the loss of protoplasm and promote plasma membrane resealing. Mutants defective in Woronin body production bleed protoplasm extensively through open septal pores (9–11), leading to defects in sporulation (9, 10) and an inability to colonize the plant host (12) in the plant pathogen, *Magnaporthe oryzae*.

Further complexity at the septal pore is revealed by thin-section electron microscopy (TEM), in which electron-dense aggregates are observed lining the rim or fully occluding the pore (13, 14). These structures show remarkable morphological variation, both between species and within species between vegetative and reproductive cell types (14, 15). However, their molecular composition remains unknown.

Here, using a bioinformatics approach that identifies related proteins based on shared composition and character, we identify a group of septal pore-associated (SPA) proteins controlling diverse aspects of septal organization and intercellular communication. These proteins are related through long intrinsically disordered domains, and in vitro assembly assays suggest an inherent tendency to aggregate. We propose that the plasticity afforded by aggregating SPA proteins allows scalable pore-templated assembly that can accommodate variation in pore diameter and convert pore-lining rings into pore-occluding plugs.

Results

MS Identifies SPA Proteins. Woronin bodies were purified from *Neurospora crassa*, and two associated proteins, NCU00627 and NCU02972, were identified by MS (Fig. 1A). We produced GFP tags at the endogenous loci (16) and found that both produce fluorescent rings lining the septal pore (Fig. 1B and C); based on their localization, we named these gene products SPA1 (NCU00627) and SPA2 (NCU02972). Both proteins also associate with Woronin bodies at the septal pore during cellular wound healing (Fig. 1B) and in cellular extracts (Fig. 1D). In vegetative hyphae, refractive structures can be observed at pores by light microscopy, and SPA-GFP signal appears to coincide with these (Fig. 1C). We also found that SPA1 rings are retained at the pore in detergent-extracted hyphal ghosts, suggesting tight linkage (Fig. 1E). In hyphae stressed by excision from the colony (*SI Materials and Methods*), SPA1-GFP produces a punctate cytosolic signal and pore rings can apparently expand to occlude the pore (Fig. 1B). This can occur in compartments throughout the agar block, suggesting that SPA assembly and pore localization are

Author contributions: J.L., C.H.K., L.P., L.W., and G.J. designed research; J.L., C.H.K., M.T., L.P., V.R., K.B.C., and G.J. performed research; C.H.K. and L.W. contributed new reagents/analytic tools; J.L., D.Y., and G.J. analyzed data; and J.L. and G.J. wrote the paper.

The authors declare no conflict of interest.

This article is a PNAS Direct Submission. H.A.B.W. is a guest editor invited by the Editorial Board.

¹To whom correspondence should be addressed. E-mail: gregory@tlil.org.sg.

This article contains supporting information online at www.pnas.org/lookup/suppl/doi:10.1073/pnas.1207467109/-DCSupplemental.

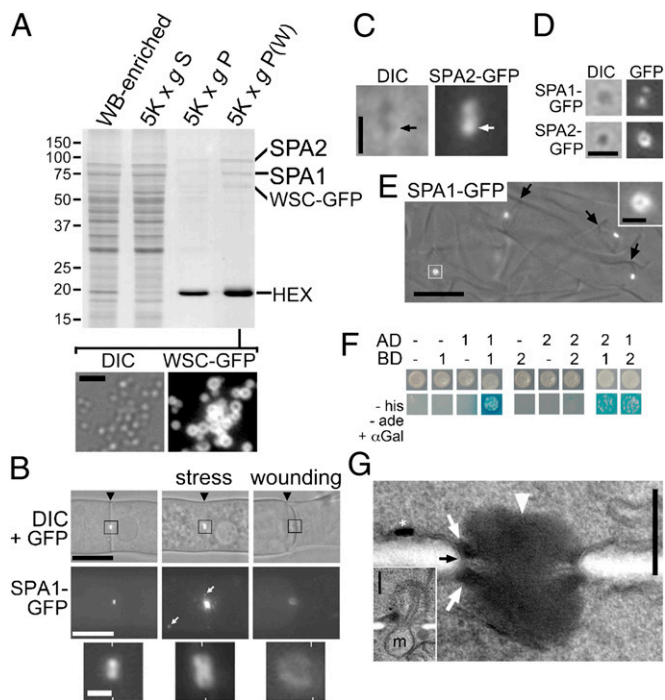


Fig. 1. Two Woronin body interacting proteins localize in rings around the septal pore. (A) Isolation of Woronin body (WB)-associated proteins. The indicated fractions were separated by SDS/PAGE. The Woronin body-specific membrane marker Woronin sorting complex (WSC) is GFP-tagged (WSC-GFP), and it allowed assessment of Woronin body enrichment during the purification process (Lower). HEX, WSC-GFP, SPA1, and SPA2 are indicated. (Scale bar: 2 μ m.) (B) SPA1 localizes at the septal pore and rearranges in stressed hyphae (stress) and during wound-induced (wounding) membrane resealing. (Bottom) Expanded views of the indicated regions are presented. (Scale bars: Upper and Middle, 5 μ m; Bottom, 1 μ m.) (C) SPA2-GFP is localized to the pore, and its fluorescence coincides with refractive structures that can be observed by differential interference contrast microscopy (DIC) (arrow). (Scale bar: 1 μ m.) (D) SPA proteins associate with Woronin bodies in cellular extracts. (Scale bar: 1 μ m.) (E) Detergent-treated cell wall ghosts retain SPA1-GFP rings. Arrows point to septa. (Scale bars: 10 μ m; Inset, 1 μ m.) (F) SPA1 and SPA2 interactions are shown by yeast two-hybrid assay. The indicated versions of the activation domain (AD) and binding domain (BD) were expressed in yeast and assayed on the indicated media. his, histidine; ade, adenine, α Gal, 5-Bromo-4-chloro-3-indoxyl- α -D-Galactopyranoside. (G) Septal pore-associated electron-dense aggregates as seen by TEM. White arrows indicate peripheral material, and the white arrowhead points to central pore-occluding material. The black arrow points to plasma membrane traversing the pore. An asterisk identifies artifact of the staining process. (Inset) Another septum from the same experiment, which is open and through which a mitochondrion (m) is trafficking. (Scale bar: 200 nm.)

regulated by a systemic response to wounding. Finally, SPA1 but not SPA2 can self-associate, and SPA1 and SPA2 interact in the yeast two-hybrid system (Fig. 1F), suggesting coassembly.

We next used TEM to examine *Neurospora* septal pore ultrastructure. Septal pores in vegetative hyphae are found in a variety of states. They can be open or occluded by electron-dense, pore-associated structures (Fig. 1G). Favorable sections of occluded pores reveal peripheral electron-dense material that is closely associated with the plasma membrane and an apparently distinct central pore-occluding material (Fig. 1G). These structures can also show symmetry in the plane of the septum and are not delimited by membranes, suggesting that they originate from the cytoplasm of both compartments. Overall, these observations are consistent with previous EM studies (13, 14).

Bioinformatics Identifies the SPA Family of Pore-Associated Intrinsically Disordered Proteins. SPA1 and SPA2 are found in diverse filamentous Ascomycetes (the clade Pezizomycotina) but do

not share primary sequence homology. BLAST searches with SPA1 identified two additional Pezizomycotina-specific proteins (SPA3 and SPA4), which share a small domain with SPA1 (Fig. S1) and GFP-SPA3 also localizes to the pore (see below).

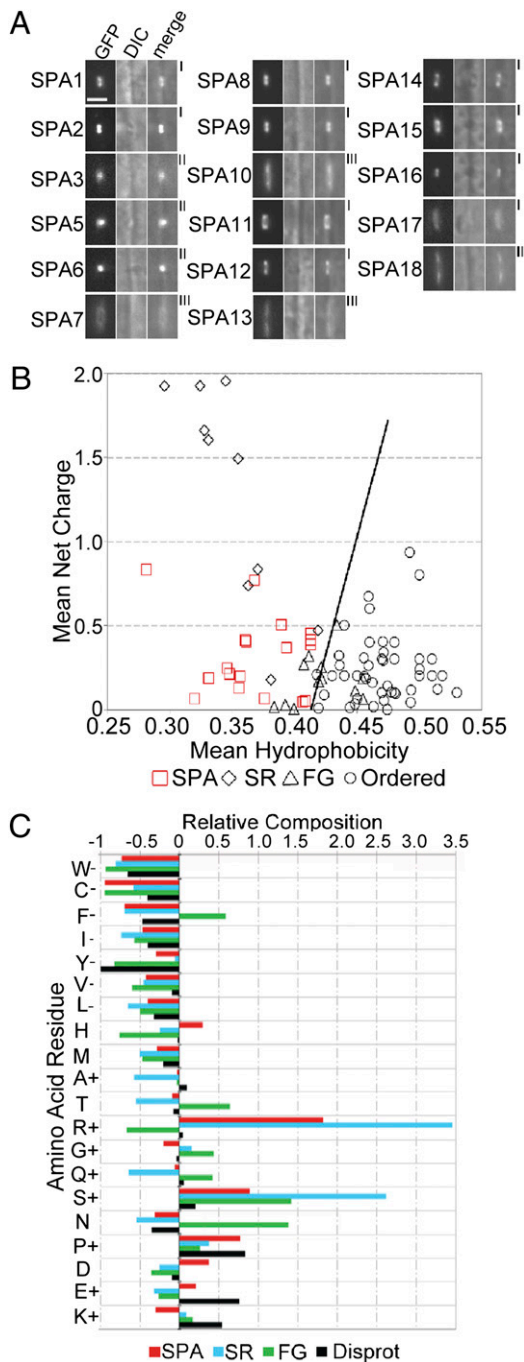


Fig. 2. SPA proteins localize to the septal pore and possess features of intrinsically disordered proteins. (A) Images show the localization of the indicated SPA proteins at the septal pore. Type I localization produces a fine ring around the septal pore rim. Type II signal emanates from the center of the septal pore, and type III localization occurs in a broad disk centered at the septal pore. DIC, differential interfering contrast microscopy. (Scale bar: 2 μ m.) (B) Charge-hydropathy analysis of SPA proteins (red \square) and folded (\circ), FG-repeat (\triangle), and SR-repeat splicing (\diamond) factors. The order/disorder boundary is indicated with a solid line. (C) Amino acid composition of disordered domains from SPA, FG-repeat (FG), SR-repeat (SR), and disordered proteins (Disprot) is shown relative to folded globular domains.

Sequence analysis revealed that these proteins are all highly charged and enriched in amino acids associated with intrinsically disordered proteins (IDPs) (17, 18). Deletion strains of these four *spa* genes did not produce obvious phenotypes, suggesting functional redundancy, and based on these observations, we reasoned that additional SPA proteins could be identified based on shared composition and character.

Using the sequence of the four SPA proteins and a machine-learning approach that was trained to recognize SPA-associated features from a total of 35 physicochemical parameters (19), candidate SPA proteins were predicted from the *Neurospora* proteome. The ranked output returned SPA1–SPA4 in the top 5 predicted SPA proteins, and after manual filtering of the output (*Materials and Methods*), we GFP-tagged the top 50 candidates. These tags, expressed from endogenous regulatory sequences, were recovered in 43 of 50 candidate genes. Based on septal pore localization, these identified 14 previously undescribed SPA proteins (Fig. 2A and Fig. S2). Among all the SPA proteins, 7 localize in rings like those observed with SPA1 and SPA2 (type I), 3 produce punctate signal from the center of the pore (type II), and 4 are found in broad and uniform pore rings (type III). Type I and type II patterns are not mutually exclusive; for example, SPA5 can be observed in both patterns. We also examined the localization of SPA1, SPA5, and SPA15 to septa of hyphae encompassing over 1 cm of apical and subapical hyphae. These data show that different SPA proteins engage newly formed pores at different times, their localization is sporadic in similarly aged septa, and pore-associated signal can increase with age (Fig. S3).

Many of the features that identify SPA proteins through machine learning are primary characteristics of IDPs. These include low mean hydrophobicity and enrichment for disorder-promoting amino acids, such as proline, serine, and arginine. Unstructured proteins are classically distinguished from folded proteins by plots of hydrophobicity vs. net charge (18). We performed charge-hydrophobicity analysis and compared SPA proteins with phenylalanine/glycine (FG)-repeat nucleoporins (FG-Nups) (20) and serine/arginine (SR)-repeat splicing factors (21), both of which possess long disordered domains. In this analysis, all 18 SPA proteins clearly fall into the disordered category (Fig. 2B). Analysis of amino acid composition further suggests that SPA proteins are IDPs (Fig. 2C). However, SPAs, FG-Nups, and SR proteins can be distinguished from one another by distinct compositional bias (Fig. 2C). SR-repeat proteins have a relatively high net charge, and this reflects enrichment for arginine, whereas SPA proteins generally possess a low mean net charge, and this reflects enrichment for arginine as well as acidic amino acids.

When subjected to BLAST analysis, many SPA proteins identify homologs in other filamentous Ascomycetes, and when conserved regions are compared with graphs of predicted disorder, many

correspond to segments of low predicted disorder (Fig. 3, green bars). Thus, in addition to extensive disordered regions, these proteins are likely to possess discreet globular domains. This pattern is observed in SPA1, SPA3, SPA4, SPA5, SPA6, SPA7, SPA9, and SPA14 (Fig. 3). Two of these are homologous to known domains: SPA14 possesses an annexin domain, and SPA5 has weak homology to the complex proteins associated with Set1p component Shg1, whereas the rest are apparently unique domains. Interestingly, homologs identified by conserved ordered domains typically retain extensive disordered regions, suggesting that disorder is maintained in evolution and is functionally important (Fig. S4). We also found that SPA2, SPA12, and SPA17 are predicted to possess long coiled-coil domains, whereas short coiled-coil domains are predicted in SPA5, SPA10, and SPA15 (Fig. 3).

Cell Wounding and Compartmental Cell Death Induce SPA Reorganization. We next examined the behavior of SPA proteins in the context of cellular wounding (Fig. S5). When hyphae are mechanically severed or lysed by hypotonic shock, a single Woronin body is typically translocated to the septal pore nearest to the point of injury and new hyphal tips are regenerated from this position (22). SPA1, SPA2, SPA9, SPA11, SPA14, and SPA15 all associate with Woronin bodies at the occluded septal pore within minutes of cellular wounding (Fig. S5A); however, with the exception of SPA9 (see below), they are not associated with Woronin bodies away from the pore. In animals, cell wounding prompts calcium-dependent annexin self-assembly on the plasma membrane to promote membrane resealing (23). Thus, in the context of Woronin body function, the annexin domain of SPA14 is likely to reveal membrane-associated calcium. This was further confirmed using the fluorescent probe chlortetracycline (24) (Fig. S5A). Finally, actin filaments (25) and GFP-MYO2 [a class V myosin and marker of the tip-localized Spitzenkörper vesicle supply center (26)] localize at the occluded pore well before new tips emerge from the septum (Fig. S5B and C). Together, these data define a dynamic wounding response involving specific SPA proteins, membrane-associated calcium, F-actin polymerization, and vesicular trafficking.

Hyphae undergo cell-to-cell fusion to promote homeostasis within the colony, and this process can also occur between individuals to produce heterokaryons containing genetically dissimilar nuclei. Cell fusion between strains that are dissimilar at specific *het* loci leads to septal pore plugging, hyphal compartmentation, and cell death in a process known as vegetative incompatibility (27, 28). We next produced incompatible reactions in strains expressing SPA1-GFP and SPA2-GFP. In these colonies, isolated compartments containing extensive SPA aggregates both at the pore and in the cytoplasm were identified (Fig. S5D), suggesting that SPA

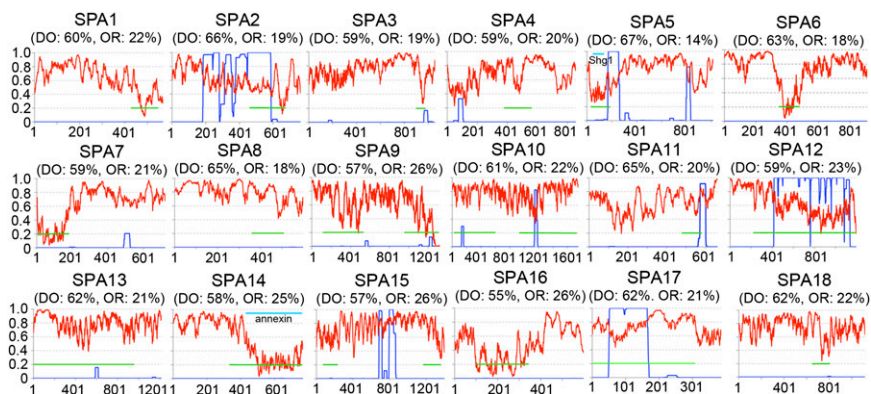


Fig. 3. Disorder, coiled-coil domains, and sequence conservation of SPA proteins. The y axis indicates the predicted probability of disorder [red line; IUPred (45)] and predicted coiled-coil domains (blue line). The x axis corresponds to amino acid sequence, and green bars indicate approximate regions of primary sequence conservation with homologous sequences from other filamentous Ascomycetes. Regions with homology to known domains [Shg1 homologous sequence in SPA5 and annexin domain in SPA14] are identified with a blue bar. DO, disordered; OR, ordered.

aggregates are effectors of the incompatible response and contribute to cellular compartmentalization by plugging septal pores.

Biochemical Analysis of SPA Protein Aggregation. We next examined SPA1 sedimentation in both WT and the Δhex mutant, which cannot make the Woronin body dense core (9). In both cases, significant amounts of SPA1 are found in the pellet after brief centrifugation at $1,000 \times g$, more sediments are found at $10,000 \times g$, and sedimentation is complete after centrifugation at $100,000 \times g$ (Fig. 4A). This indicates that SPA1 is found in heterogeneously sized aggregates whose formation is independent of HEX. When exposed to various chemical treatments, SPA1 aggregates are resistant to Triton X-100 (Fig. 4A) but are solubilized in urea and SDS (Fig. 4B), indicating assembly through noncovalent protein-protein interactions.

SPA disordered domains are enriched for charged amino acids, and SPA5 possesses an extreme version of this architecture, possessing extensive arginine/aspartic acid (RD) repeats (Fig. S6). To

examine the potential of SPA proteins to self-assemble in vitro, we expressed various SPA disordered (SPA1^{DO} and SPA5^{DO}) and ordered (SPA1^{OR}, SPA5^{OR}, SPA7^{OR}, and SPA16^{OR}) domains in *Escherichia coli*. Both disordered domains and the SPA1^{OR} domain were found exclusively in bacterial inclusion bodies, whereas the SPA5^{OR}, SPA7^{OR}, and SPA16^{OR} domains could be purified as soluble proteins. Insoluble SPA domains were next purified under denaturing conditions and dialyzed into a physiological buffer to examine self-assembly (Fig. 4C). In this system, SPA1^{OR}, SPA1^{DO}, and SPA5^{DO} all aggregate to produce spherical assemblies (Fig. 4C and D) that can be pelleted by low-speed centrifugation (Fig. 4C) and dissolved by SDS at room temperature (Fig. 4D). By contrast, controls consisting of lysozyme; BSA; and disordered domains from the yeast gel forming FG-Nup, Nsp1p (29), and the *Neurospora* SOFT protein (*Discussion*) remain soluble when subjected to the same procedure (Fig. 4C), indicating that these assay conditions do not generally result in protein aggregation. SPA5^{DO} aggregates are especially large and appear to flatten between the slide and coverslip, suggesting that they are soft gels. This was confirmed by micromanipulation with a glass needle, which can penetrate and pull extensions from SPA5 assemblies (Fig. 4E and Movie S1).

We next examined SPA1^{DO}, SPA5^{DO}, and SPA1^{OR} aggregates by FTIR spectroscopy (Fig. S7). Deconvolution followed by curve fitting suggests that SPA1^{OR} aggregates are composed of 71% α -helix, 22% β -strand, and 7% unordered structure; SPA1^{DO} aggregates contain 55% α -helix, 31% β -strand, and 14% unordered structure; and SPA5^{DO} aggregates consist of 13% α -helix, 39% β -strand, and 47% unordered structure. This structural composition is distinct from well-characterized amyloid aggregates, which typically possess a preponderance of β -structural conformation (30). Having defined both SPA1^{OR} and SPA1^{DO} domains as aggregating, we tested the ability of these to promote pore localization independently by replacing one or the other region with GFP. This analysis shows that both domains are capable of independently driving pore localization (Fig. 4F) and suggests redundant aggregation-dependent mechanisms for pore localization of SPA1.

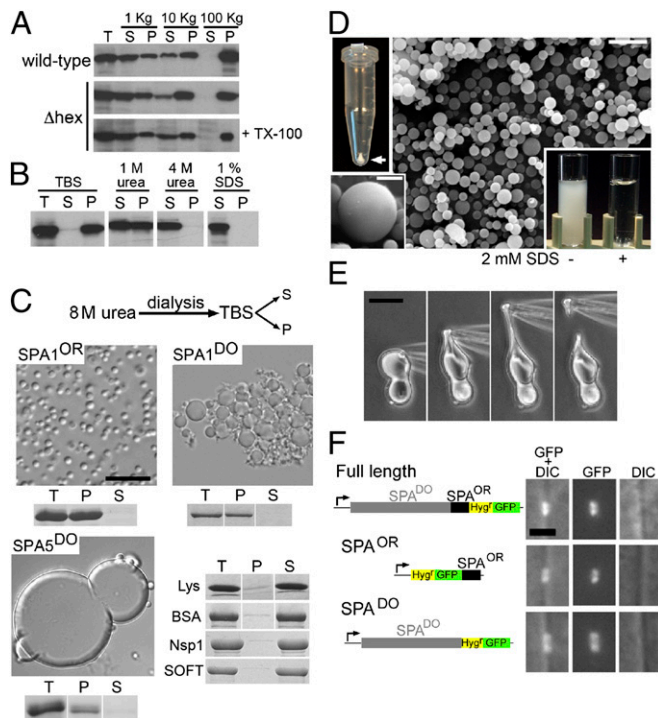
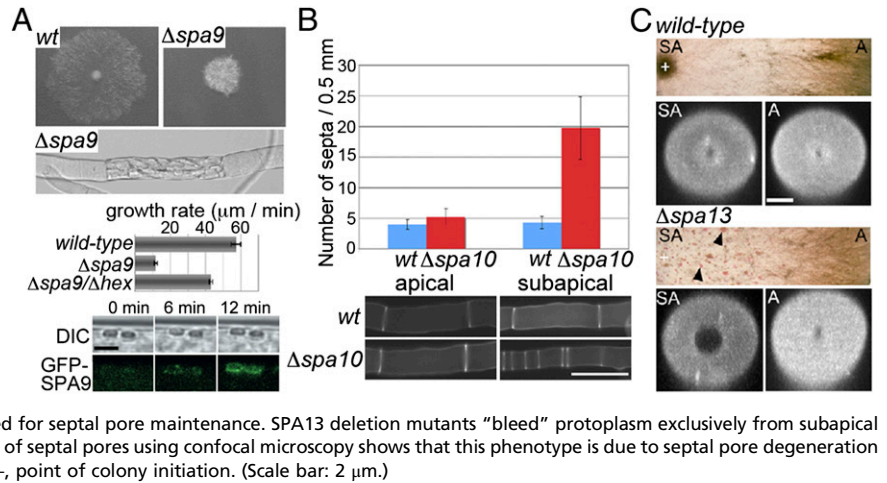


Fig. 4. Biochemical analysis of SPA aggregates and in vitro assembly of SPA domains. (A) Cytosolic extract from WT and Δhex mutant hyphae was fractionated by centrifugation into supernatant (S) and pellet (P) fractions in the absence and presence of Triton X-100 (+TX-100), and SPA1 distribution was determined by Western blotting. T, total extract. (B) Stability of SPA1 aggregates. A $10,000 \times g$ pellet fraction was resuspended in the indicated chemicals, followed by centrifugation to produce supernatant and pellet fractions. SPA1 distribution was determined by Western blotting. (C) His-tagged versions of SPA1^{OR}, SPA1^{DO}, and SPA5^{DO} domains were purified under denaturing conditions and dialyzed into Tris-buffered saline, followed by microscopic examination and fractionation into pellet and supernatant fractions by centrifugation. Lysozyme, BSA, SOFT^{DO}, and Nsp-1 subjected to the same conditions produced no visible aggregates and remained in the S fraction. DO, disordered; OR, ordered. (D) SPA1^{OR} aggregates were collected by centrifugation (arrow) and examined by SEM. Insets show enlarged SPA sphere (Lower Left) and disassembly of concentrated SPA1^{OR} aggregates in 2 mM SDS (Lower Right). (Scale bars: 10 μm ; Inset, 2 μm .) (E) SPA5^{DO} aggregates have gel-like properties. Individual images correspond to frames extracted from Movie S1. (Scale bar: 50 μm .) (F) Both SPA1^{OR} and SPA1^{DO} domains are capable of recognizing the septal pore. (Left) Cartoon shows the genomic structure produced by marker fusion tagging. (Right) Localization is shown. DIC, differential interfering contrast microscopy. (Scale bar: 2 μm .)

SPA Proteins Regulate Diverse Aspects of Septal Function and Biogenesis. Deletion of three SPA proteins produced distinct loss-of-function phenotypes that manifest at the level of the septum. The *spa9* deletion strains produce intrahyphal hyphae that originate from the septum and present a dramatic reduction in radial colony growth (Fig. 5A). Aberrant activation of Woronin bodies is known to produce these phenotypes (31), suggesting that this could be the root cause of the *spa9* defect. Indeed, abolishing Woronin body function by deletion of *hex* suppresses the *spa9* growth defect (Fig. 5A). Moreover, a functional GFP-SPA9 fusion protein rapidly redistributes to the surface of Woronin bodies when hyphae are wounded (Fig. 5A); like the aggregation of SPA1, this can occur in compartments well removed from sites of hyphal injury. Together, these observations suggest that SPA9 is formally an inhibitor of Woronin body activation, although the precise mechanism of its action remains to be determined.

Hyphal tip extension occurs at the colony periphery, and periodic septation partitions the hypha into compartments. Compared with WT hyphae, the *spa10* deletion strain has a normal distribution of septa in apical compartments. However, in subapical hyphae, increased numbers of septa are observed (Fig. 5B), suggesting that SPA10 function is required to suppress septation in older hyphae. SPA13 regulates yet another feature of the septum: Hyphae of *spa13* deletion strains rupture and accumulate puddles of protoplasm in subapical but not apical regions of the colony (Fig. 5C). We examined the diameter of septal pores by laser scanning confocal microscopy and Z-sectioning. In WT hyphae, pores formed in apical cells retain their diameter as they age. By contrast, *spa13* mutant pores have a normal diameter when they form but become aberrantly enlarged as they age (Fig. 5C), and this explains why these strains bleed protoplasm despite possessing

Fig. 5. SPA proteins regulate Woronin body function, septation, and septal pore stability. (A) SPA9 controls Woronin body release. (Top) *spa9* deletion strain exhibits impaired colony growth and intra-hyphal hyphae. (Middle) Deletion of HEX eliminates Woronin bodies and suppresses the growth defect (graph). DIC, differential interfering contrast microscopy. (Bottom) Localization of GFP-SPA9 to cortical Woronin bodies during the systemic response to injury. (Scale bar: 1 μm .) (B) SPA10 regulates septation. The *spa10* deletion mutants develop normal numbers of septa in apical compartments but elaborate abnormally high numbers of septa as the hypha ages. Septa were counted in the apical and subapical compartments ~ 1 cm behind the colony growth front. Septal numbers are quantified in the graph (Upper), and representative hyphae are shown (Lower). (Scale bar: 10 μm .) (C) SPA13 is required for septal pore maintenance. SPA13 deletion mutants “bleed” protoplasm exclusively from subapical regions of the colony (arrowheads), and reconstruction of septal pores using confocal microscopy shows that this phenotype is due to septal pore degeneration in old regions of the colony. A, apical; SA, subapical; +, point of colony initiation. (Scale bar: 2 μm .)



Woronin bodies (Movie S2). This pore degeneration occurs mainly in large primary hyphae engaged in tip-directed trafficking of protoplasm but not in similarly aged and less active secondary hyphae. Thus, SPA13 is required to maintain the integrity of pores stressed over time by extensive cell-to-cell transport.

Discussion

Cell-to-cell channels evolved independently in all multicellular eukaryotic phyla to allow direct communication between neighboring cells and are known to play important roles in developmental patterning and physiological coupling of tissues in animals and plants (3). Although fungal cell-to-cell channels are known to promote cellular cooperativity (28), little is known about the protein constituents of the pore and their role in organizing fungal tissues. Our study identifies the fungal septal pore as a complex cellular address and focal point for the assembly of functionally diverse IDPs that regulate intercellular communication and various aspects of septal organization.

SPA proteins are defined by disordered domains and shared biases in amino acid composition but are diverse in terms of both localization (Fig. 2) and function (Fig. 5). Type I and type II SPA proteins appear to be involved in pore-rim lining and occlusion (Fig. 1 and Fig. S5), and they provide a Woronin body-independent mechanism for gating the pore that can respond to physiological signaling (Fig. S5). Understanding how the extent of SPA aggregation is controlled will be an interesting area for further investigation. A subset of SPA proteins also associates with Woronin bodies during wound-induced membrane resealing (Fig. S5), suggesting that they function like mortar to consolidate the Woronin body/septal pore complex during early stages of membrane resealing. Most of these SPA proteins do not associate with Woronin bodies away from the pore, suggesting that proximity to the pore is required to license Woronin bodies for SPA assembly.

SOFT is a cytoplasmic protein required for fungal cell-to-cell fusion, which has previously been localized to septal pore plugs (32, 33). The N-terminal domain of SOFT is predicted to be disordered (Fig. S8) but presents biases in amino acid composition distinct from those observed for SPA proteins, such as enrichment for glutamine (Fig. S8). SOFT also scored poorly in the SPA prediction (position 1,327 of 9,834) and does not form aggregates in our *in vitro* system (Fig. 4C). Interestingly, α -helical coiled coils have recently been shown to modulate the aggregation of Q/N-rich prions and PolyQ proteins (34), indicating that β -sheet and coiled-coil promoted aggregation are not mutually exclusive. Coiled-coil domains are also predicted in SPA proteins (Fig. 3) and could function to promote pore localization of other proteins, such as SOFT.

Disordered domains of SPA1 and SPA5 are inherently prone to aggregate (Fig. 4). SPA1 and SPA2 interact (Fig. 1F) but do not display dependency in their ability to localize to the septal pore.

This, together with the independent ability of SPA1^{OR} and SPA1^{DO} domains to promote pore localization (Fig. 4F), is consistent with assembly of type I and type II SPA proteins through a network of redundant interactions. We suggest that pore lining and occlusion by SPA proteins consist of aggregate nucleation at the pore rim, followed by growth through homo- and heterotypic interactions of SPA disordered domains. In *Neurospora*, septal pore diameter varies between 200 and 500 nm, and it scales with hyphal diameter (13). The structural plasticity afforded by SPA aggregation may provide a unique solution to the problems presented by variable pore diameter and requirements for pore gating.

Disordered proteins possess a low content of hydrophobic amino acids typically required for the formation of globular protein folds, and are thus unstructured in isolation (18, 35). However, IDPs are recognized to function in the formation of intermolecular complexes, where disordered domains can attain a precise fold on binding to their partner molecules in a process known as coupled binding and folding (36). This flexibility allows binding to multiple targets, as in hub proteins (37, 38), and is believed to confer a unique combination of specificity with weak and reversible binding.

Long disordered domains have previously been associated with self-assembled high-ordered protein aggregates. FG-Nups form multivalent interactions between FG-repeat sequences to produce a hydrogel composed of random coils (20, 29). SPA proteins bear interesting parallels with FG-Nups. Both groups of proteins assemble at pores, possess long disordered domains (20) (Fig. 4), and self-assemble to form high-order aggregates *in vitro* (29) (Fig. 4). In FG-Nups, intermolecular contacts are promoted by FG-mediated hydrophobic interaction (29). Based on their amino acid composition and enrichment for both acidic and basic amino acids (Fig. 2), we suggest that SPA assembly is mediated through electrostatic attractive interactions, hydrogen bonding, and weak hydrophobic interactions. The failure of disordered domains from SOFT and Nsp1p to aggregate under our assay conditions (Fig. 4C) further indicates that aggregation of SPA disordered domains is specific and dependent on their unique composition.

SPA aggregates produced *in vitro* are spherical (Fig. 4C) and SDS-sensitive (Fig. 4A and D), and FTIR spectra suggest that they are composed primarily of α -helical structures for SPA1^{DO} and SPA1^{OR} and disordered structures for SPA5^{DO} (Fig. S6). Therefore, these aggregates appear to be distinct from amyloid aggregates, which form SDS-resistant fibrils (39) and contain a preponderance of β -sheet structure. The appearance and physical properties of SPA aggregates (Fig. 4) suggest liquid-gel phase separation, which has been invoked to explain the formation of subcellular compartments, such as various RNA/protein bodies (40) and signaling complexes (41). In the cellular context, phase separation has recently been shown to depend critically on a high degree of multivalency in interacting proteins (41). In this regard,

as demonstrated here for certain SPA unstructured regions, long disordered domains, with their ability to adopt flexible conformations and make large numbers of intermolecular contacts, may be especially well-suited to participate in this form of cellular compartmentation. RD repeats like those found in SPA5 are also found in certain animal proteins associated with RNA splicing (42). Moreover, SR splicing factors are IDPs (21), and phosphorylation of serine in RS repeats is expected to make them behave more like RD repeats. This raises the intriguing possibility that SPA-like assembly may be involved in the compartmentation of cellular RNA metabolism.

Materials and Methods

Neurospora Growth and Genetic Manipulation. *Neurospora* strains were grown and maintained on synthetic Vogel's N medium as previously described (31). Candidate *spa* genes were GFP-tagged using marker fusion tagging in either FGSC9719 or FGSC9720 background as previously described (16). Deletion mutants (43) in *spa* genes were obtained from the Fungal Genetics Stock Center.

Machine Learning. Sirius Prediction System Builder (version 2.2) (19) was used to identify potential SPA proteins based on their physicochemical properties. The analysis used 35 dimensions consisting of composition of individual amino acids and 15 physicochemical properties. The initial four SPA proteins were used as a positive training set, and the predicted *Neurospora* proteome was used as a negative set. The χ^2 value for each was determined, and the top 10 dimensions for the SPA proteins were as follows: (i) mean hydrophobicity, (ii) net charge, (iii) magnitude of net charge, (iv) composition of arginine, (v) mean net charge, (vi) magnitude of mean net charge, (vii)

composition of ordered amino acids, (viii) composition of phenylalanine, (ix) composition of cysteine, and (x) difference between ordered and disordered amino acids. The top 100 proteins from the ranked output were manually annotated using BLAST searches, and their phylogenomic distribution was determined based on previous studies (44). Short peptides, *Neurospora* orphans, and genes with known functions were not tagged (Fig. S2). Additional information on methods used to predict disorder, coiled-coil domains, and charge-hydropathy analysis is provided in *SI Materials and Methods*.

Protein Expression, Purification, and in Vitro Aggregation. His-tag fusion proteins were expressed in *E. coli* BL21 (DE3) and purified under denaturing conditions (Qiagen). Proteins were dialyzed using either a Slide-A-Lyzer MINI Dialysis unit or Slide-A-Lyzer Dialysis Cassette G2 (Pierce) in a stepwise fashion from 8 M urea to Tris-buffered saline buffer [150 mM NaCl, 10 mM Tris (pH 7.4)]. Following dialysis, the samples were examined by light microscopy and were then centrifuged at 10,000 \times g for 10 min at 4 °C to determine the appearance and physical properties of aggregates, respectively. The total, supernatant, and pellet fractions were subjected to SDS/PAGE, and proteins were stained with Coomassie Brilliant Blue (Fig. 4C).

Details about Woronin body purification and FTIR are provided in *SI Materials and Methods*.

ACKNOWLEDGMENTS. We thank Ouyang Xuezhong for help with EM and Jingru Chan, Fangfang Liu, Yanfen Lu, and Seng Kah Ng for help with gene tagging. We acknowledge the use of deletion mutants generated by National Institutes of Health Grant P01 GM068087 "Functional Analysis of a Model Filamentous Fungus." D.Y. acknowledges funding by the biomedical Research Council, A*STAR of Singapore (R154000373305). Research in the G.J. group is supported by the Singapore Millennium Foundation and Temasek Life Sciences Laboratory.

- Bonner J (1999) The origins of multicellularity. *Integrative Biology (Camb)* 1(1):27–36.
- Rokas A (2008) The molecular origins of multicellular transitions. *Curr Opin Genet Dev* 18:472–478.
- Zambryski P, Crawford K (2000) Plasmodesmata: Gatekeepers for cell-to-cell transport of developmental signals in plants. *Annu Rev Cell Dev Biol* 16:393–421.
- Xu XM, Jackson D (2010) Lights at the end of the tunnel: New views of plasmodesmal structure and function. *Curr Opin Plant Biol* 13:684–692.
- Goodenough DA, Paul DL (2009) Gap junctions. *Cold Spring Harb Perspect Biol* 1:a002576.
- Stajich JE, et al. (2009) The fungi. *Curr Biol* 19(18):R840–R845.
- Jedd G (2011) Fungal evo-devo: Organelles and multicellular complexity. *Trends Cell Biol* 21(1):12–19.
- van Peer AF, et al. (2009) The septal pore cap is an organelle that functions in vegetative growth and mushroom formation of the wood-rot fungus *Schizophyllum commune*. *Environ Microbiol* 12:833–844.
- Jedd G, Chua NH (2000) A new self-assembled peroxisomal vesicle required for efficient resealing of the plasma membrane. *Nat Cell Biol* 2:226–231.
- Tenney K, et al. (2000) Hex-1, a gene unique to filamentous fungi, encodes the major protein of the Woronin body and functions as a plug for septal pores. *Fungal Genet Biol* 31:205–217.
- Maruyama J-I, Juvvadi PR, Ishi K, Kitamoto K (2005) Three-dimensional image analysis of plugging at the septal pore by Woronin body during hypotonic shock inducing hyphal tip bursting in the filamentous fungus *Aspergillus oryzae*. *Biochem Biophys Res Commun* 331:1081–1088.
- Soundararajan S, et al. (2004) Woronin body function in *Magnaporthe grisea* is essential for efficient pathogenesis and for survival during nitrogen starvation stress. *Plant Cell* 16:1564–1574.
- Trinci AP, Collinge AJ (1973) Structure and plugging of septa of wild type and spreading colonial mutants of *Neurospora crassa*. *Arch Mikrobiol* 91:355–364.
- Read ND, Beckett A (1996) Ascus and ascospore morphogenesis. *Mycol Res* 100:1281–1314.
- Kimbrough JW (1994) *Ascomycete Systematics: Problems and Perspectives in the Nineties*, ed Hawksworth DL (Plenum, New York), pp 127–141.
- Lai J, et al. (2010) Marker fusion tagging, a new method for production of chromosomally encoded fusion proteins. *Eukaryot Cell* 9:827–830.
- Uversky VN, Dunker AK (2010) Understanding protein non-folding. *Biochim Biophys Acta* 1804:1231–1264.
- Uversky VN (2011) Intrinsically disordered proteins from A to Z. *Int J Biochem Cell Biol* 43:1090–1103.
- Koh CH, Lin S, Jedd G, Wong L (2009) Sirius PSB: A generic system for analysis of biological sequences. *J Bioinform Comput Biol* 7:973–990.
- Denning DP, Patel SS, Uversky V, Fink AL, Rexach M (2003) Disorder in the nuclear pore complex: The FG repeat regions of nucleoporins are natively unfolded. *Proc Natl Acad Sci USA* 100:2450–2455.
- Haynes C, Iakoucheva LM (2006) Serine/arginine-rich splicing factors belong to a class of intrinsically disordered proteins. *Nucleic Acids Res* 34:305–312.
- Trinci APJ, Collinge AJ (1974) Occlusion of the septal pores of damaged hyphae of *Neurospora crassa* by hexagonal crystals. *Protoplasma* 80(1):57–67.
- Bouter A, et al. (2011) Annexin-A5 assembled into two-dimensional arrays promotes cell membrane repair. *Nat Commun* 2:270.
- Silverman-Gavrila LB, Lew RR (2002) An IP3-activated Ca²⁺ channel regulates fungal tip growth. *J Cell Sci* 115:5013–5025.
- Riedl J, et al. (2008) Lifeact: A versatile marker to visualize F-actin. *Nat Methods* 5:605–607.
- Steinberg G (2007) Hyphal growth: A tale of motors, lipids, and the Spitzenkörper. *Eukaryot Cell* 6:351–360.
- Fleissner A, Simonin AR, Glass NL (2008) Cell fusion in the filamentous fungus, *Neurospora crassa*. *Methods Mol Biol* 475:21–38.
- Glass NL, Rasmussen C, Roca MG, Read ND (2004) Hyphal homing, fusion and mycelial interconnectedness. *Trends Microbiol* 12(3):135–141.
- Frey S, Richter RP, Görlich D (2006) FG-rich repeats of nuclear pore proteins form a three-dimensional meshwork with hydrogel-like properties. *Science* 314:815–817.
- Toyama BH, Weissman JS (2011) Amyloid structure: Conformational diversity and consequences. *Annu Rev Biochem* 80:557–585.
- Liu F, et al. (2008) Making two organelles from one: Woronin body biogenesis by peroxisomal protein sorting. *J Cell Biol* 180:325–339.
- Fleissner A, Glass NL (2007) SO, a protein involved in hyphal fusion in *Neurospora crassa*, localizes to septal plugs. *Eukaryot Cell* 6:84–94.
- Maruyama J-I, Escaño CS, Kitamoto K (2010) AoSO protein accumulates at the septal pore in response to various stresses in the filamentous fungus *Aspergillus oryzae*. *Biochem Biophys Res Commun* 391:868–873.
- Fiumara F, Fioriti L, Kandel ER, Hendrickson WA (2010) Essential role of coiled coils for aggregation and activity of Q/N-rich prions and PolyQ proteins. *Cell* 143:1121–1135.
- Dunker AK, Silman I, Uversky VN, Sussman JL (2008) Function and structure of inherently disordered proteins. *Curr Opin Struct Biol* 18:756–764.
- Wright PE, Dyson HJ (2009) Linking folding and binding. *Curr Opin Struct Biol* 19:31–38.
- Demarest SJ, et al. (2002) Mutual synergistic folding in recruitment of CBP/p300 by p160 nuclear receptor coactivators. *Nature* 415:549–553.
- Oldfield CJ, et al. (2008) Flexible nets: Disorder and induced fit in the associations of p53 and 14-3-3 with their partners. *BMC Genomics* 9(Suppl 1):S1.
- Serio TR, et al. (2000) Nucleated conformational conversion and the replication of conformational information by a prion determinant. *Science* 289:1317–1321.
- Hyman AA, Brangwynne CP (2011) Beyond stereospecificity: Liquids and mesoscale organization of cytoplasm. *Dev Cell* 21(1):14–16.
- Li P, et al. (2012) Phase transitions in the assembly of multivalent signalling proteins. *Nature* 483:336–340.
- Perutz M (1994) Polar zippers: Their role in human disease. *Protein Sci* 3:1629–1637.
- Colot HV, et al. (2006) A high-throughput gene knockout procedure for *Neurospora* reveals functions for multiple transcription factors. *Proc Natl Acad Sci USA* 103:10352–10357.
- Kasuga T, Mannhaupt G, Glass NL (2009) Relationship between phylogenetic distribution and genomic features in *Neurospora crassa*. *PLoS ONE* 4:e5286.
- Dosztányi Z, Csizmok V, Tompa P, Simon I (2005) IUPred: Web server for the prediction of intrinsically unstructured regions of proteins based on estimated energy content. *Bioinformatics* 21:3433–3434.